A novel electrochemical procedure for grown of bimetallic metal–organic framework (Ni/Zn-MOF) and its derived hydroxide@C onto Ni foam as binder-free high performance battery-type electrodes for supercapacitors

Qichao Song
Wuxi Institute of Technology
Chunguang Yang (ch.mingya@gmail.com)
Wuxi Institute of Technology https://orcid.org/0000-0003-4922-020X

Research Article

Keywords: Supercapacitors, Electrochemical fabrication, Ni,Zn-MOF, Synergistic effect, Specific capacity

Posted Date: March 16th, 2021

DOI: https://doi.org/10.21203/rs.3.rs-282285/v1

Abstract

Todays, metal-organic frameworks (MOFs) and their derived structures have been extensively investigated as the novel electrode materials in energy storage area due to their stable porous architectures and exceptionally large specific surface area. In this study, bimetallic Ni,Zn-MOF is synthesized onto Ni foam *via* a novel indirect cathodic electrodeposition method for the first time. After that, the fabricated Ni,Zn-MOFs onto Ni foam was converted to corresponding bi-metal hydroxide@C/Ni foam through direct chemical treating with 6M KOH solution. The obtained Ni,Zn-MOFs/NF and $Ni_{2-x}Zn_x(OH)_2$@C/NF electrodes are characterized through XRD, FT-IR, FE-SEM and EDS analyses. These analyses results confirmed deposition of well-defined crystalline porous sheet-like structures of $Ni_{3-x}Zn_x(BTC)_2$ deposited onto Ni foam, where the hydroxide@C electrode was also exhibited similar morphology. As the binder-free electrode, the as-prepared Ni,Zn-MOF@Ni foam exhibited the superior storage capacities of 356.1 mAh g^{-1} and 255.5 mAh g^{-1} as well as good cycling stabilities of 94.2 % and 84.5 % after 6000 consecutive charge/discharge cycles at the current densities of 5 and 15 A g^{-1}, respectively. On the other hand, Ni,Zn-MOF derived hydroide@C/Ni foam presented the superior capacities of 545 mAh g^{-1} and 406 mAh g^{-1} as well as proper cycle lifes of 91.8 % and 78.3 % after 6000 cycling at the applied loads of 5 and 15 A g^{-1}, respectively. Based on these findings, both of these fabricated battery-type electrodes are introduced as the promising candidates for use in energy storage devices.

1. Introduction

In the recent years due to the growing demand for energy and problems related with fossil fuels such as the constant change in world prices, concerns about the scarcity of fossil fuels and global warming due to greenhouse gas emissions and with emerging the high power application that required high power and energy efficiency, reliability and long discharging cycle life, the development of renewable and environmentally friendly energy and, of course energy storage technologies for the practical applications, has received much attention since the early 1990s [1, 2]. Improving the efficiency of energy storage systems, as an important part of energy consumption management, has always been the focus of research by scientists around the world. Among many energy storage systems, supercapacitors have received a lot of attention due to their high power density, long service life, fast charge/discharge, good cyclic stability, excellent intrinsic safety and wide operating temperature [3]. Possibility for design and development of new electrochemical capacitors with high efficiency are needed high performance electrode materials. Currently, there are many different types of capacitors that categorized by the dielectric properties and/or its physical state. Each type has its own unique characteristics and applications ranging from small capacitors for electronics devices to large power capacitors used in high-voltage power device [4]. Electrochemical capacitors (ECs) that categorized in the two main groups of electrochemical double layer capacitor (EDLC) and pseudocapacitor [4] are a special kind of capacitors based on charging and discharging at the electrode–electrolyte interface of high surface area materials, such as porous carbon derived materials [5, 6], graphene-based structures, conducting polymers and s [7–9].

Among all the electrode materials used, metal-organic frameworks (MOFs) are a new class of porous materials prepared by chemical interaction of organic linkers and metal ions or clusters [10–12]. MOFs have also employed for chemical separations, drug delivery, electrocatalysis, fluorescence and electrochemical studies as well as energy storage purposes (supercapacitors, lithium-ion batteries), photocatalyst, gas sensing, water treatment, solar cells, and carbon dioxide capture [11]. Because of the unique properties such as tunable pore sizes, high porosity, extremely high surface area and ordered crystalline structures, MOFs have attracted great attention in the last two decades [2, 11]. However, the direct application of MOFs in electrode materials is limited by the poor electroconductibility, large steric hindrance and the chemical/mechanical stability [13–15]. Hence, it is essential to explore new strategy to enhance the electrochemical performance of MOFs. MOFs materials with single metallic element always exhibit poor performance for the inactivated sites and undesirable structure [16]. Yang *et al.* synthesized a layered structure Ni-based MOF with capacitances of 1127 and 668 F g^{-1} at rates of 0.5 and 10 A g^{-1}, respectively [17]. Bimetallic MOFs with two different kinds of central metal ions could provide improved electrochemical performance for SC [16, 18]. The synergistic effect of the mixed metal ions can effectively enhance the conductivity and specific area of MOFs, which makes the MOF-electrode exhibit superior specific capacitance and preferable cycling life [19]. Yang *et al.* [20] reported synthesis of a Zn-doped Ni-MOF with capacitances of 1620 and 860 F g^{-1} were achieved at 0.25 and 10 A g^{-1}, respectively, and the retention was kept at 91% even after 3000 cycles for MOF sample with a Zn/Ni of 0.26. Chen *et al.* [21] have prepared bimetallic Ni/Co-MOFs with nano-sheet assembled flower-like morphology with high specific capacitance of 1220.2 F g^{-1} at 1 A g^{-1} and high capacitance retention of 87.8% after 3000 cycles. Xia *et al.* have developed a kind of Ni/Co-MOF with flake-assembled spherical microstructures, which had a capacitance of 530.4 F g^{-1} at 0.5 A g^{-1} and almost no capacity attenuation after 2000 charge/discharge cycles [22]. Bimetallic MOFs with homogeneous distribution of two kinds of metal nodes could be utilized as ideal templates to construct bimetallic oxides with controllable composition. Micro- and/or nanopores in MOFs can be retained after post treatment, which benefits improving ion mobility and high specific capacitance of supercapacitors. MOF-derived oxides structures are the promising candidate for supercapacitor electrode material due to its layered structure, low cost and environmental friendly physicochemical feature [23].

In most of these studies, solvothermal and hydrothermal methods have been used for synthesis of MOFs materials. However, these methods often contain multi-step and complex processing procedures or high-cost techniques, leading to low reproducibility and they often are time and resource-consuming [24–25]. Compared with the conventional methods, electrochemical method is considered as one of the most promising method to prepare MOF thin films and coatings because this method does not require complex preparation steps and has a short growth time and the possibility of the controlling the phase, morphology and size of the MOF products by altering the synthesis parameters. Also electrochemical synthesis allows the large-scale production of MOFs in powder form [26].

In this paper, we report simple deposition of a well-structured bimetallic Ni,Zn-MOF though indirect cathodic electrochemical procedure onto Ni-foam support and its chemical treating in basic solution to

convert bimetal hydoxide@C active material. The fabricated electrodes were directly used as binder-free capacitor electrode, which have advantageous such as additive-free, possibility of bulk production and porous texture.

2. Experimental Procedure

2.1. Sample preparation

For fabrication of the Ni,Zn-MOF onto Ni-foam cathode, an indirect cathodic electrodeposition procedure was employed. In this deposition protocol, a typical two-electrode electrochemical cell composed of Ni foam (SA = 2 cm^2) as the cathode side and two-parallel graphite plates as the anode side (SA = 6 cm^2) were used. The electrolyte solution was prepared with dissolving the 0.25 *g* BTC, 0.15 g $Ni(NO_3)_2$, 0.1 g $Zn(NO_3)_2$ and 0.2g $NaNO_3$ in 100 mL of double distilled water. The electrodeposition process was carried out at the current load of 25 mA/cm^2 for 10 min. The deposition temperature and pH of the electrolyte solution were 25 ^oC and 5.5, respectively. After depositions, the Ni-foam cathode was washed several times with the double distilled H_2O and heat-treated at 80 ^oC for 6h. The fabricated Ni,Zn-MOF/Ni foam was then applied as ready-to-use binder-free electrode in the charge storage tests. To prepare MOF-derived hydroxide electrode, the Ni,Zn-MOF onto Ni foam was directly putted in 6M KOH solution for 12h, where the solution was agitated during the reaction time. After that, the Ni-foam electrode was immerged into deionized water for 24 h and then heat-treated at 80 ^oC for 4h. The powder form of Ni,Zn-MOF was also synthesized by the similar cathodic procedure using Ni plate as the cathode side. In which, the film formed onto Ni foil was removed and heat-treated at the 80 ^oC for 6 h. The synthesized sample was named as Ni,Zn-MOF powder.

2.2. Sample characterizations

FE-SEM (model Mira 3-XMU) was applied to determine the morphology characteristics and elemental mapping of the fabricated Ni,Zn-MOF/NF and its derived hydroxide/NF electrodes. X-ray diffraction (XRD) analyses was performed through X'Pert PRO MRD instrument. FT-IR spectra of pure BTC and the synthesized MOF powder were taken *via* a Bruker Vector 22 FT-IR spectrometer (in the range of 400–4000 cm^{-1}).

2.4. Electrochemical tests

Electrochemical tests were carried out using potentiostat/galvanostat Eco Chemie instrument with specifications AUTOLAB®, Model: PGSTAT 30. In the electrochemical set-up, the fabricated Ni,Zn-MOF/NF or MOF-derived hydroxide/Ni foam was connected to working line of PGSTAT 30. The Pt rod and Ag/AgCl were also connected to the counter and reference positions, respectively. The electrolyte of the electrochemical cell was selected to be 2M potassium hydroxide. CV graphs were recorded within the potential domain of -0.1 and 0.6 V vs. Ag/AgCl (for the fabricated Ni,Zn-MOF/Ni foam electrode) and −0.3 and 0.7 V vs. Ag/AgCl (for MOF-derived hydroxide/Ni foam). Notably, mass loads of Ni,Zn-MOF and

MOF-derived hydroxide formed onto Ni-foam cathodes were respectively found to be 5.6 mg and 4.1 mg. The capacity values delivered by both fabricated working electrodes were calculated from the CV diagrams using the following expression [24]:

$$\mathrm{C}(mAh/g) = \frac{\mathrm{Q}}{2\mathrm{m}*3.6}\mathrm{andQ} = \int_{\mathrm{v1}}^{\mathrm{V_2}} I(V)\,dV (1)$$

In this relation, C (*m*Ah/g) is the specific capacity, Q is total charge (Coulombs), ΔV is the applied potential window in volt unit, *m* is mass of the Ni,Zn-MOF and MOF-derived hydroxide (*g*), and I(V) is the measured currents (A). The GCD digrams were also recorded at the current loads between 1 to 30 A g^{-1} in the potential window of -0.1 to 0.45 V and the specific capacities of each electrode were obtained *via* relation (2) [25]:

$$C = \frac{Q}{m \times 3.6} andQ = \int_{t1}^{t2} idt (2)$$

where C is the stored charge by WE electrode in mAh/g unit, I is the current load in A unit, ΔV is the potential window (0.55 V), Δt is the time of a discharge branch in second unit and *m* is mass of the electrodeposited active material (g). Electrochemical impedance spectroscopy (EIS) profiles were obtained at the frequencies ranging from 100 to 0.001 kHz at OCP potential of 5 mV.

3. Results And Discussion

Fig. 1 shows XRD patterns of the Ni,Zn-BTC/Ni foam electrode and the Ni,Zn-MOF powder. Nickel foam (NF) with 3D macro-porous structure, high mechanical strength, flexibility, high electrical conductivity and relatively high specific surface areas is proper support as current collector for the capacitor electrode. Its macro-porous channels with several hundred micrometers pore size could provide enhanced mass transport for the involved electrochemical processes [26-27]. As seen in Fig. 1a, for the fabricated Ni,Zn-MOF/NF electrode, three peaks with maximum intensity are observed at the diffraction angles 44.57°, 52.24 ° and 76.16 ° which are related to (111), (200) and (220) planes of Ni foam. With respect to high intensity of diffraction peaks of nickel-foam substrate, the diffraction related to MOF deposited onto Ni-foam have disappeared as the background peaks. However, Ni,Zn-MOF deposited onto Ni-foam presents four main peaks located at 8.53°, 11.41° and 13.56° (Fig. 1a) which are analogous to those previously reported for Ni,Zn-MOF [28-29]. Fig. 1b shows the powder XRD diffraction pattern of the prepared Ni,Zn-MOF powder. From the XRD pattern, it is obvious that the Ni,Zn-MOF powder exhibited crystalline structure with peaks position similar to those observed for the Ni,Zn-MOF/NF electrode. This indicates that the prepared Ni,Zn-MOF in both forms of powder and thin film shows the similar topological structure, which has formed by connection of the metal ions with BTC ligands [30-31].

The XRD pattern of the MOF-derived hydroxide/Ni foam electrode is also presented in Fig. 1c. In this pattern, tree sharp diffractions related to Ni foam are clearly seen at 2θ of 44.57°, 52.24 ° and 76.16 °, [illegible] planes of Ni foam. The diffraction peaks related to Ni,Zn-

hydroxides are also seen at the 2θ of 9.58 º, 19.26 º, 22.32 º, 37.45 º, 38.51 º, 47.26 º and 57.9 º, which are due to the crystal planes of (001), (002), (201), (110), (102) and (103), respectively (Fig. 1c).

Fourier transformation infrared (FT-IR) spectroscopy was also employed to characterize the prepared Ni,Zn-MOF sample. FTIR spectra of the pure benzene,3-tricarboxylic acid (H_3BTC) and Ni,Zn-MOF powders are shown in Fig. 2. For both samples, the intensive band at 3417 cm^{-1} is due to the stretching vibrations of water molecules (OH vibrations) [32]. The IR spectrum of H_3BTC (Fig. 2a) showed peaks at 1722 cm^{-1} and 1277 cm^{-1} corresponding to stretching vibrations of C=O and C-O, respectively, indicating the presence of carboxylic acid groups in BTC structure [32]. The symmetric and antisymmetric stretching vibrations of O-C-O groups are in the range of 1350–1620 cm^{-1} [33]. More precisely, the bands at 1620, 1577, 1448 and 1382 cm^{-1} are respectively related to the asymmetric and symmetric stretching vibrations of the carboxylate groups in BTC [32]. Compared with IR spectrum of pure BTC in Fig. 2a, it was found that although there is no significant changes in the peak positions for the Ni,Zn-MOF powder sample (Fig. 1b), several new IR bands are appeared at the low wavenumbers of 1000 cm^{-1}. This is due to the adsorption of metal ions to the structure of BTC through its carboxylic functional groups. As a result, the peaks related to Ni-O are observed at 830 and 689 cm^{-1} and Zn-O bond vibration is found at 520 cm^{-1} [34]. Therefore, it was concluded that Ni and Zn cations have been successfully introduced into the framework of BTC linkers to form Ni,Zn-MOF structure.

FE-SEM images of the prepared Ni,Zn-MOF/Ni electrode are given in Fig. 3. The three dimensional and open pore structure of the Ni foam support are clearly seen in Figs. 3a,b, which the Ni,Zn-MOF deposits are fully covered the Ni foam framework and some pores.

The Ni/Zn-MOF deposit exhibits a flower-like morphology with three-dimensional spatial structure like as petals (Fig. 3b). The observed petals are consisting of multilayered nanosheets and irregular distribution with thickness of ~500 nm, where their lateral surfaces become relatively smooth (Fig. 3d). This morphology can be strongly influenced by the method of electrochemical synthesis and the simultaneous presence of nickel and zinc metallic ions, because the structure observed in this paper is significantly different from the structures reported in other articles [31,35]. It is well known that the Ni,Zn-BTC coordination complex can form 3D polymeric chains via the strong π–π interaction or hydrogen bonding between the ligands could hold the chains together to form 3D network [36].

Fig. 4 shows the elemental mapping and energy dispersive X-ray analysis (EDX) of the Ni,Zn-MOF/Ni foam. In the elemental mapping profiles, it is seen that the carbon and oxygen elements (Figs. 4b,c) have completely similar pattern of the MOF morphology observed in Fig. 4a. This observation verified that the BTC linker formed the building blocks of the fabricated Ni,Zn-MOF. The synthesized Ni,Zn-MOF only have C, O, Ni and Zn elements with the weight percentages of 33.82 %, 40.18%, 15.81 % and 10.19 %, respectively (Figs. 4a-d). These elements are uniformly distributed in the MOF framework (Figs. 4d,e). EDX results showed that the ratio of Ni/Zn in the fabricated MOF sample is 3:2 (Fig. 4e).

The Ni,Zn-MOF derived hydroxide onto Ni-foam electrode was also analyzed by FE-SEM technique to observe its morphology. Fig. 5 presents FE-SEM images of the MOF-derived hydroxide onto Ni-foam support. In FE-SEM image of Fig. 5a, the Ni-foam framework and open pore is easily seen and it is also observed that the derived hydroxide is present at all surfaces of Ni foam (Fig. 5b). Similar to pristine MOF, the derived hydroxide has three-dimensional flower-like morphology (Fig. 5b). The observed 3D flower has composed of the plates with several micrometers in sizes and relative porous texture (Figs. 5c,d).

Fig. 6 shows the elemental mapping and energy dispersive X-ray analysis (EDX) of the Ni,Zn-MOF-derived hydroxide onto Ni foam. The hydroxide formed onto Ni-foam exhibited C, O, Ni and Zn elements in its composition. The presence of nickel, zinc and oxygen (Figs. 6c-e) is corresponded to the $Ni_{2-x}Zn_x(OH)_2$ chemical composition of the prepared hydroxide after chemical treating with strong KOH solution. The carbon presence is also give that the hydroxide formed onto Ni foam has been carbon particles on its backbone. Hence, the chemical formula of the $Ni_{2-x}Zn_x(OH)_2$@C could be ascribed to the MOF-derived hydroxide onto Ni-foam. EDAX data in Fig. 6f indicates that the fabricated material onto Ni-foam has the atomic percentages of 45.9 % carbon, 37.38% oxygen, 10.13 % nickel and 6.59 % zinc atoms (Fig. 6f). These atomic percentages indicated that the ratio of Ni/Zn in the fabricated MOF sample is about 3:2 (Fig. 6f) and hence the chemical formula of $Ni_{1.5}Zn_{0.5}(OH)_2$@C is predicted for the MOF-derived hydroxide onto Ni-foam.

After characterization of the electrodeposited films of Ni,Zn-MOF and its derived hydroxide onto the conductive nickel-foam support, their electrochemical performances as binder-free capacitive electrode were evaluated through CV, GCD and EIS tests. Fig. 7a shows CV plots of the binder-free pristine Ni,Zn-MOF/Ni foam and its derived $Ni_{1.5}Zn_{0.5}(OH)_2$@C/Ni foam electrodes at the scan rate of 5 mV/s. Notably, the applicable potential window for the fabricated Ni,Zn-MOF/Ni foam and $Ni_{1.5}Zn_{0.5}(OH)_2$@C/Ni foam electrodes were 0–0.55V and -0.2–0.6 V vs. Ag/AgCl, respectively. In CV curve of an ideally reversible system, the oxidation and reduction peaks have same potential difference at various scan rates based on the number of electrons involved in the electrochemical reaction. Thus, in quasi-reversible systems the oxidation peak moves to more positive potentials and reduction peak moves to more negative potentials due to the presence of kinetic barriers in charge transfer processes at the electrode/electrolyte interface when the scan rate is increase. For both fabricated electrodes (Fig. 7a), the observed pair of redox peaks within the CV curves was ascribed to Ni(II)↔Ni(III) and Zn(II) ↔Zn(III) (i.e. M–O/M–O–OH, M=Zn or Ni) during anodic scan which were reversed during cathodic potential sweep [37-39]. Additionally, it is seen that by increasing the scan rate, the specific capacitances are decreased (Figs. 7b,c) due to the inaccessibility of some active sites within the fabricated active material onto Ni-foam for electrolyte ion diffusion.

Fig. 8 exhibits the plots of i_p vs $\nu^{1/2}$ and i_p vs ν for the Ni,Zn-MOF/NF and MOF-derived hydroxide@C/NF electrodes, which manifesting that the currents are linearly related with the square root of scan rate for both fabricated electrodes. The peak current of a battery-type electrode material is linearly related to square root of the scanning rate ($i_p \sim v^{1/2}$), whereas a capacitor-type material exhibited linear current

response relation on the scan rate (i∼v). So, it can be said that both fabricated electrodes i.e. Ni,Zn-MOF/Ni foam $Ni_{1.5}Zn_{0.5}(OH)_2$@C/Ni foam store charges through typical battery-type process [40,41]. The capacity values of the fabricated electrodes were calculated through Eq. (1) and the results are given in Fig. 7d. It was calculated that Ni,Zn-MOF/Ni foam electrode is capable to deliver capacity values of 396, 367, 345, 304, 268, 227 and 202 mAh g^{-1} at the scan rates of 5, 10, 20, 50, 100, 200 and 300 mV/s, respectively. And, the $Ni_{1.5}Zn_{0.5}(OH)_2$@C/Ni foam electrode showed specific capacities of 593.8, 546.7, 515.4, 331.8, 472.1, 422.5, 370.3 and 324.2 mAh g^{-1} at the scan rates of 5, 10, 20, 50, 100, 200 and 300 mV/s, respectively. These data indicated that the prepared bimetallic Ni,Zn-MOF/NF electrode retained more than 52 % of its primary capacity by increasing the scan rate from 5 to 300 mV/s, which signified a proper high-rate capability of the fabricated MOF electrode. Furthermore, $Ni_{1.5}Zn_{0.5}(OH)_2$@C/Ni foam electrode served its 54.59% of its initial storage at the high applied scan rate of 300 mV/s, verifying its proper high-rate capacitive performance.

Fig. 9 exhibits galvanostatic charge/discharge curve of the fabricated Ni,Zn-MOF/NF and $Ni_{1.5}Zn_{0.5}(OH)_2$@C/Ni foam electrodes at the different current loads of 1, 3, 5, 7, 10, 15, 20 and 30 A/g. The GCD curves of both electrodes showed the nearly non-linear charge-discharge behavior within the applied potential window, which is in good agreement with CV curves in Figs. 7b,d. These GCD profiles implicated battery-type behavior of the fabricated bimetallic Ni,Zn-MOF/NF and $Ni_{1.5}Zn_{0.5}(OH)_2$@C/Ni foam. In all GCD curves, one couple of charge/discharge plateau is observed, which is originated from Faradic reactions of conversion of Ni (II) to Ni (III) and Zn (II) to Zn (III), which implicated a battery-like characteristics of prepared electrodes (Figs. 9b,c). From the GCD curves, columbic efficiency of both electrodes were calculated and plotted in Fig. 9d. The calculations showed that the columbic efficiencies change from 99.7% to 79.1 for Ni,Zn-MOF/NF electrode and from 98.9% to 76.5% for $Ni_{1.5}Zn_{0.5}(OH)_2$@C/Ni foam electrode by increasing the applied current load from 1 A/g to 30 A/g (Fig. 9d). These results verified the proper battery-type storage performances of both prepared electrodes.

GCD curves were also utilized to estimate the specific capacities of the bimetallic MOF and hydroxide material at the different current densities, as presented in Fig. 9e. The specific capacity values of this pristine bimetal MOF/NF electrode were calculated to be as high as 442.9, 396.5, 356.1, 331.8, 297.4, 255.6, 238.3 and 209.6 mAh g^{-1} at the current densities of 1, 3, 5, 7, 10, 15, 20 and 30 A g^{-1}, respectively. The MOF-derived hydroxide/Ni foam electrode is also presented specific capacities of 637, 605, 545, 497, 455, 406, 406, 352 and 324 mAh g^{-1} at the current densities of 1, 3, 5, 7, 10, 15, 20 and 30 A g^{-1}, respectively. These data verified that MOF-derived hydroxide active material onto Ni foam has larger charge storage than those of pristine MOF onto Ni foam, which maybe related to the high density of active sites in the hydroxide electrode as compared with those of pristine MOF electrode, where most weight of the pristine electrode is composed by organic linker. Furthermore, these data indicate that the capacity values were gradually falls by increasing of the applied current density. The major reason for this reduction trend is that the electrolyte ions cannot fully access to the active sites of the electrode bulk material under high current densities and only outer parts/surfaces of the active electrode material are

igh current densities. Hence, the electrochemical contribution

of both Ni^{2+} and Zn^{2+} centers into the faradic reactions for both electrodes is limited at the high-rate discharging conditions, resulting the reduced specific capacities delivered by the Ni,Zn-MOF/NF electrode [42-44]. However, the high-rate performances of 50.46% and 49.18% were respectively observed for Ni,Zn-MOF/NF and Ni,Zn-hydroxide@C/NF electrodes with increasing the applied current load from 1 to 30 A/g. For comparison of the capacitive performance of our prepared MOF and derived hydroxide active material with those reported in literature, some data are listed in **Table 1**. Comparison of the capacitive performance of our fabricated bimetal Ni,Zn-MOF/NF with those reported for single metal MOF electrode (i.e. Ni-MOF with Cs=334 mAh/g at 1 A/g, rate capability=49% and capacity retention=42.8 % after 2500 cycles at 10 A g^{-1} [37]) proved the better charge storage ability of the mixed Ni^{2+}/Zn^{2+}-based MOF electrode as a result of the synergetic effects within the fabricated MOF structure [38-41]. In fact, the incorporation or doping of zinc within Ni-MOF affects both the ionic and electronic conductivity, which results in better electrode utilization and the improvement of reaction kinetics, which is vital factor for any supercapacitor electrode material [42-45]. Furthermore, large operational potential window is another key factor for a supercapacitor, which lead to obtain high energy density values [44-46]. In fact, the wider potential window will cause an incredible enhancing the delivered energy densities. Compared with the Ni/Co-MOF (ΔV=0.45V [38]), Ni-MOF (ΔV=0.4 V [39]), Ni-MOF (ΔV=0.4V [44]), Zn/Co-MOF (ΔV=0.41V [43]), Zn/Ni-MOF (ΔV=0.5 V [44]), Ni/Zn-MOF ((ΔV=0.35 V [45]) and Ni/Zn-MOF ((ΔV=0.5V [46]) reported up now, the potential window of our fabricated Ni,Zn-MOF electrode (ΔV=0.6 V) was expanded, further indicating its better electrochemical performance as supercapacitor electrode. As seen in **Table 1**, the Ni,Zn-MOF electrode fabricated by our simple electrochemical method exhibits better specific capacity, high-rate capability and capacity retention as compared with those reported for Ni-based bimetal MOF electrodes in literature [37-46], which can be related to its layered three-dimensional spatial petal-like structure (Figs. 3,5), proper distribution of metal cation centers (Figs. 4,6) and suitable contact to Ni-foam support (Fig. 12).

The cycling performance is also a critical parameter to evaluate the charge storage performance of a supercapacitor. The cyclability of the fabricated pristine MOF electrode was also tested at the current loads of 5 and 15 A g^{-1} and the obtained results are presented in Fig. 10. The first ten cycles within the 6000 GCD cycling of the fabricated MOF/Ni foam electrode at the current load of 5 and 15 A/g are given in Figs. 10a,c. It is seen that the fabricated electrode exhibited a well-defined battery-type performance during the 6000 cycling tests. Through the discharge times obtained from Figs. 10a,c and using Eq. (2), the specific capacities of the Ni,Zn MOF/NF electrode were calculated at the cycle numbers of 1, 100, 200, 300, …. and 6000. The obtained capacity values were plotted against the cycle number, which are represented in Figs. 10b,d. The capacity retention or stability values at the applied charge/discharge currents were also calculated using the obtained capacity data at the above mentioned cycles (i.e. capacity retention (%)=$[C_n/C_1]\times100$, where C_n is the capacity of electrode in n^{th} cycle). Figs. 10b,d show the capacity retentions (%) versus the cycle number at both current load of 5 and 15 A/g. Based on the calculated capacity data, it was found that the specific capacity of the fabricated electrode is reduced from 356.5 mAh/g (for 1^{th} cycle) to 334.9 mAh/g (for 6000^{th} cycle) when current load was 5 A/g, as seen

at the Ni,Zn MOF/NF electrode is exhibited 255.6 mAh/g at

the fist cycle of GCD test with current load of 15 A/g, and 215.9 mAh/g at the end of 6000 cycling, as given in Fig. 10d. Also, it was revealed that our prepared electrode is capable to serve 94.1% and 84.5% of its initial capacity values after 6000 cycling at the current loads of 5 and 15 A/g, respectively (Figs. 10b,d). The cycling data of the fabricated MOF-derived hydroxide/Ni foam electrode is also presented in Fig. 11. Based on the GCD curves of this electrode at the current loads of 5 and 15 A/g (Fig. 11a,c), the two important parameters of capacitance values in each cycle and also capacity retention during the 6000 cycling process were calculated and the obtained data were plotted in Fig. 11b,d. It was observed that the $Ni_{1.5}Zn_{0.5}(OH)_2$@C/Ni foam electrode exhibits capacity values of 501.2 mAh/g and 318.1 mAh/g after 6000 cycles at the currents of loads of 5 and 15 A/g (Figs. 11b,d). Also, the capacity retentions or cycle lives of 91.9% and 78.3 % were respectively calculated for $Ni_{1.5}Zn_{0.5}(OH)_2$@C/Ni foam at these applied charge-discharging loads (Figs. 11b,d). Comparing these capacity retentions with those reported for other MOF-based electrodes listed in **Table 1** indicated that our fabricated electrode has a superior cycling ability. This good cycle life at the high current densities could be related to its appropriate electrochemical stability and also its good physical contact to the current collector support (nickel foam), which maybe originate from the direct electrochemical growth of active electrode material (i.e. Ni,Zn-MOF and $Ni_{1.5}Zn_{0.5}(OH)_2$@C) as well as its unique morphology, self-assembling, and proper distribution onto the surface of Ni-foam (Figs. 3-6).

To further verification of the observed high-capacitive performance of the fabricated electrodes, electrochemical impedance spectroscopy (EIS) at the frequency of $0.01–10^5$ Hz was recorded and its result is shown in Fig. 12. As presented in inset of Fig. 12, the EIS curve could be well-fitted with an equivalent circuit consisting of solution resistance (R_s), faradaic capacitance (C_F), Warburg resistance (W) and charge transfer resistance (R_{ct}). In the low-frequency range, both electrodes exhibit nearly straight line, ascribing to the diffusive resistance for the electrodes. Furthermore, diameter of the semicircle in the medium frequency could be used to estimate charge transfer resistance of the fabricated electrodes. In the high frequency region, intercept of the real impedance is equal to the equivalent series resistance (ESR), which are sum of the internal resistance of the electrode, the solution resistance as well as resistances of all contacts through the impedance measurement. This parameter determines the rate of charging/discharging of the electrode. R_s and R_{ct} quantities were measured to be 1.4 Ω and 0.72 Ω, respectively. The low ESR and R_{ct} quantities further manifested the high performance of the fabricated electrodes for supercapacitor applications.

4. Conclusion

In summary, a bimetallic MOF/Ni foam electrode consisting of nickel and zinc elements was successfully synthesized by a facile electrochemical deposition route. Then, it was converted to $Ni_{1.5}Zn_{0.5}(OH)_2$@C/Ni foam through chemical treating in 6M KOH solution. The fabricated materials were applied as the binder-free supercapacitor electrodes. The as-prepared Ni,Zn-MOF and its derived hydroxide material had self-assembly petal-like structures, which respectively showed a battery-type charge storage behavior with 537 mAh g^{-1} at 1 A g^{-1} and excellent capacity retentions of

94.2 % and 91.9 % after 6000 cycles at 5 A g^{-1}. The facile electrochemical route followed by chemical treating used here could be readily used for fabrication of other mixed metal MOFs and derived hydrixude@C electrodes for supercapacitor applications. More generally, by selecting of appropriate metal cations, it would be possible to synthesize various bi-metal MOFs onto any conductive support as binder-free ready-to-use electrode for energy storage aims.

References

[1] H. Wang, Q.L. Zhu, R. Zou, Q. Xu, Chem. **2**, 52 (2017)

[2] H.B. Wu, X.W.D. Lou, Sci. Adv. **3**, 9252 (2017)

[3] V. Bon, Curr. Opinion Green Sustainable Chem. **4**, 44 (2017)

[4] M. Lu, Supercapacitors: Materials, Systems, and Applications. John Wiley & Sons. (2013)

[5] J. Li, Y. Gao, K. Han, J. Qi, M. Li, Z. Teng, Scientific Reports **9**, 1 (2019)

[6] Y. Cheng, L. Wu, C. Fang, T. Li, J. Chen, M. Yang, Q. Zhang, J. Mater. Res. Technol. **9**, 3261 (2020)

[7] Q. Ke, J. Wang, J. Materiomics **2**, 37 (2016)

[8] Q. Meng, K. Cai, Y. Chen, L. Chen, Nano Energy **36**, 268 (2017)

[9] F. Shi, L. Li, X.L. Wang, C.D. Gu, J.P. Tu, RSC Adv. **4**, 41910 (2014)

[8] M. Aghazadeh, I. Karimzadeh, A. Ahmadi, M.R. Ganjali, J. Mater. Sci.: Mater. Electron. **29**, 14567 (2018).

[9] C. An, Y. Zhang, H. Guo, Y. Wang, Nanoscale Adv. **1**, 4644 (2019)

[10] M.A.A.M. Abdah, N.H.N. Azman, S. Kulandaivalu, Y. Sulaiman, Mater. Design **186**, 108199 (2020)

[11] T. Rasheed, K. Rizwan, M. Bilal, H. Iqbal, Molecules **25**, 1598 (2020)

[12] S.T. Meek, J.A. Greathouse, M.D. Allendorf, Adv. Mater. **23**, 249 (2011)

[13] M. Ding, X. Cai, H.L. Jiang, Chem. Sci. **10**, 10209 (2019)

[14] C. Wang, X. Liu, N.K. Demir, J.P. Chen, K. Li, Chem. Soc. Rev. **45**, 5107 (2016)

[15] S.M. Moosavi, P.G. Boyd, L. Sarkisov, B. Smit, ACS Central Sci. **4**, 832 (2018)

[16] L. Chen, H.F. Wang, C. Li, Q. Xu, Chem. Sci. **11**, 5369 (2020)

[17] J. Yang, P. Xiong, C. Zheng, H. Qiu, M. Wei, J. Mater. Chem. A **2**, 16640 (2014).

[18] Y. Jiao, J. Pei, D. Chen, C. Yan, Y. Hu, Q. Zhang, G., Chen, J. Mater. Chem. A **5**, 1094 (2017)

[19] J.Y. Xue, C. Li, F.L. Li, H.W. Gu, P. Braunstein, J.P. Lang, Nanoscale **12**, 4816 (2020)

[20] J. Yang, C. Zheng, P. Xiong, Y. Li, M. Wei, J. Mater. Chem. A **2**, 19005 (2014)

[21] C. Chen, M.K. Wu, K. Tao, J.J. Zhou, Y.L. Li, X. Han, L. Han, Dalton Transactions **47**, 5639 (2018)

[22] H. Xia, J. Zhang, Z. Yang, S. Guo, S. Guo, Q. Xu, Nano-Micro Lett. **9**, 1 (2017)

[23] S. Wu, J. Liu, H. Wang, H. Yan, Int. J. Energy Res. **43**, 697 (2019)

[24] S. Zhou, Y. Wei, L. Zhuang, L.X. Ding, H. Wang, J. Mater. Chem. A **5**, 1948 (2017)

[25] T.R. Van Assche, N. Campagnol, T. Muselle, H. Terryn, J. Fransaer, J.F. Denayer, Microporous Mesoporous Mater. **224**, 302 (2016)

[26] M.M. Li, Cathodic electrodeposition of metal-organic frameworks (Doctoral dissertation, Massachusetts Institute of Technology (2015)

[27] N.K. Chaudhari, H. Jin, B. Kim, K. Lee, Nanoscale **9**, 12231 (2017)

[28] Z. Zhang, Y. Chen, S. He, J. Zhang, X. Xu, Y. Yang, F. Nosheen, F. Saleem, W. He, X. Wang, Angewandte Chemie Int. **53**, 12517 (2014)

[29] N. Zhang, C. Huang, P. Tong, Z. Feng, X. Wu, L. Zhang, J. Chromatography A **1556**, 37 (2018)

[30] X. Zhang, Y. Sui, F. Wei, J. Qi, Q. Meng, Y. Ren, Y. He, J. Mater. Sci.: Mater. Electron. **30**, 18101 (2019)

[31] M. Yang, Q. Bai, Colloids Surf. A **582**, 123795 (2019)

[32] S. Alizadeh, D. Nematollahi, J. Am. Chem. Soc. **139**, 4753 (2017)

[33] W.W. Lestari, I.D. Winarni, F. Rahmawati, In IOP Conference Series: Mater. Sci. Engin. **172**, 012064 (2017)

[34] D.R. Paul, S. Gautam, P. Panchal, S.P. Nehra, P. Choudhary, A. Sharma, ACS Omega **5**, 3828 (2020)

[35] R. Song, L. Hou, Y. Wang, Y. Li, X. Wang, Y. Zang, Y. Zang, X. Wang, S. Yan, Anal. Methods **9**, 3914 (2017)

[36] P. Zarabadi-Poor, R. Marek, ACS Sustainable Chem. Engin. **6**, 15001 (2018)

[37] X. Zhang, Y. Sui, F. Wei, J. Qi, Q. Meng, Y. Ren, Y. He, J. Mater. Science: Mater. Electron. **30**, 18101 (2019)

[38] C. Xu, Y. Feng, Z. Mao, Y. Zhou, L. Liu, W. Cheng, J. Wang, H. Shi, X. Liu, J. Mater. Science: Mater. Electron. **30**, 19477 (2019)

[39] M. Azadfalah, A. Sedghi, H. Hosseini, J. Mater. Science: Mater. Electron. **30**, 12351 (2019)

[40] P. Simon, Y. Gogotsi, B. Dunn, Science **343**, 1210 (2014)

[41] Y. Gogotsi, R.M. Penner, ACS Nano **12**, 2081 (2018)

[42] H. Xia, J. Zhang, Z. Yang, S. Guo, S. Guo, Q. Xu, Nano-Micro Letters **9**, 43 (2017)

[43] X. Zhang, J. Wang, X. Ji, Y. Sui, F. Wei, J. Qi, Q. Meng, Y. Ren, Y. He, D. Zhuang, J. Mater. Science: Mater. Electron. **31**, 16260 (2020)

[44] Y. Jiao, J. Pei, D. Chen, C. Yan, Y. Hu, Q. Zhang, G. Chen, J. Mater. Chem. A **5**, 1094 (2017)

[45] J. Yang, C. Zheng, P. Xiong, Y. Li, M. Wei, J. Mater. Chem. A **2**, 19005 (2014)

[46] Y. Chen, D. Ni, X. Yang, C. Liu, J. Yin, K. Cai, Electrochim. Acta **278**, 114 (2018)

Figures

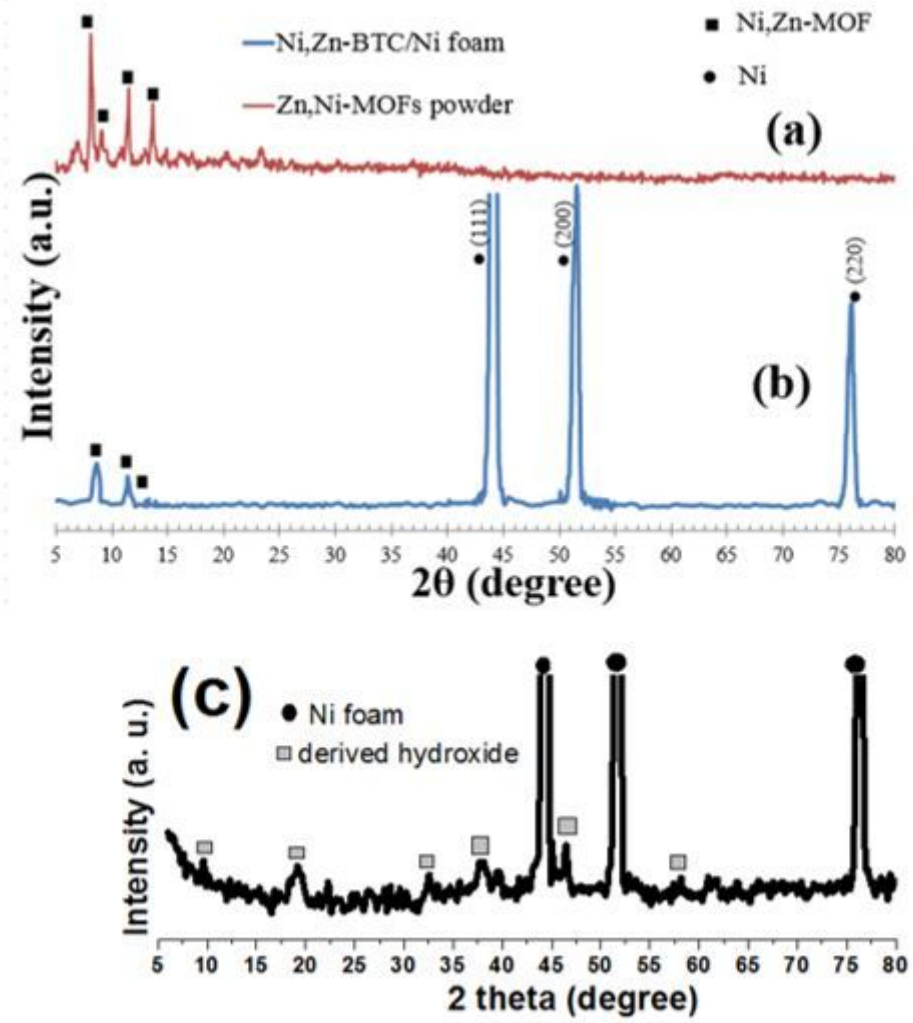

Figure 1

XRD patterns of the synthesized (a) Ni,Zn-MOF powder, (b) Ni,Zn-MOF/Ni foam electrode and (c) the MOF-derived hydroxide/Ni foam electrode.

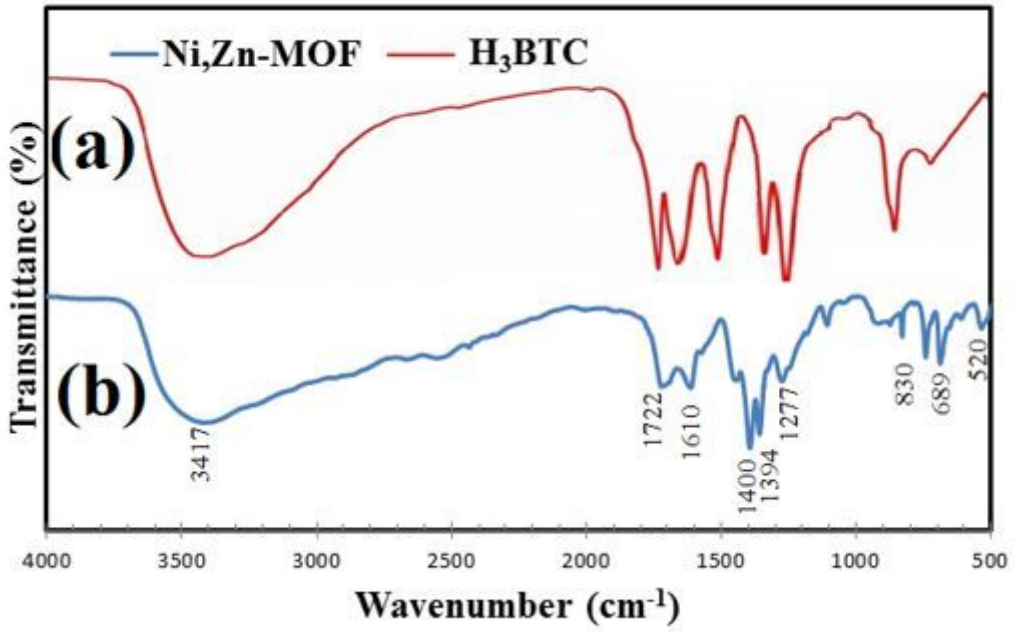

Figure 2

IR spectra of (a) pure BTC and (b) the electrochemically prepared Ni/Zn-MOF powders.

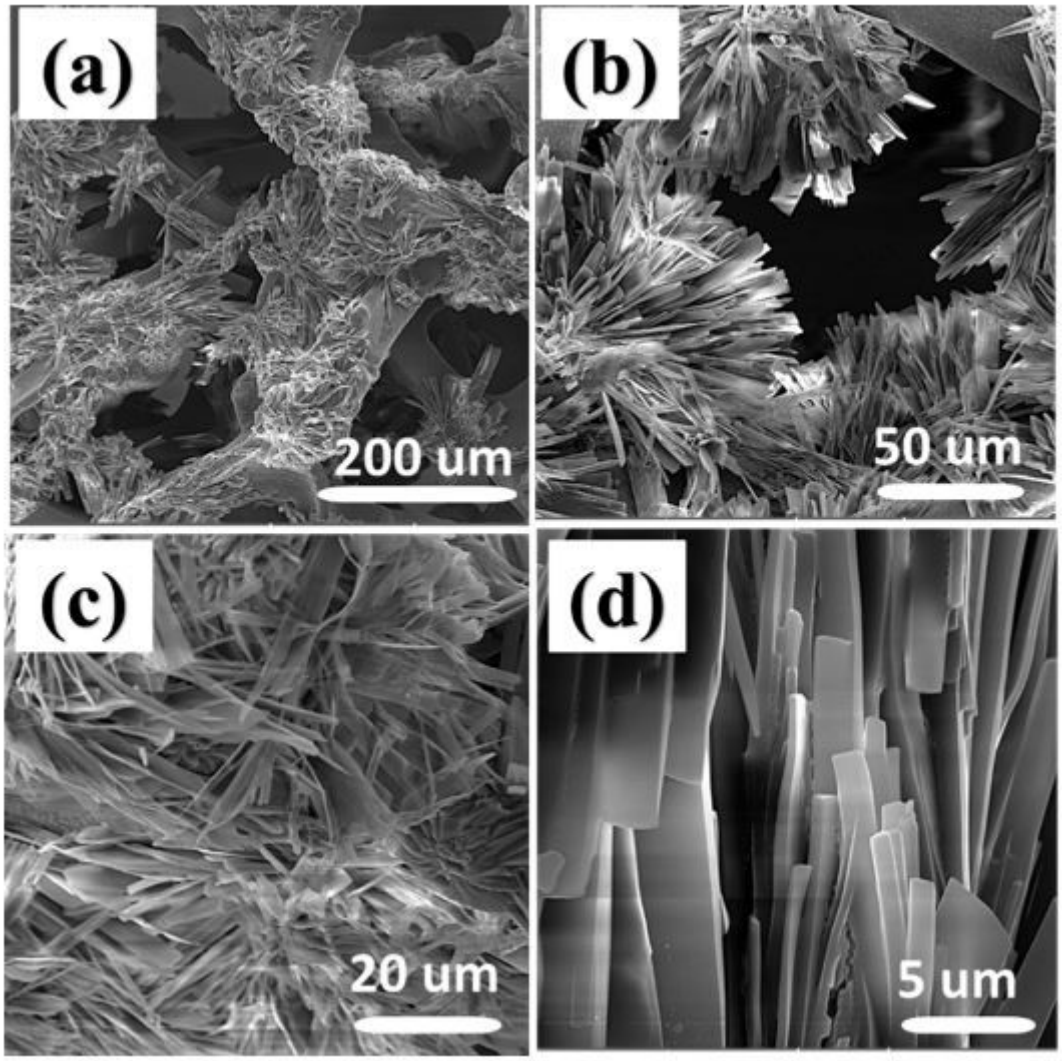

Figure 3

FE-SEM images of the Zn,Ni-MOF deposited onto Ni-foam support.

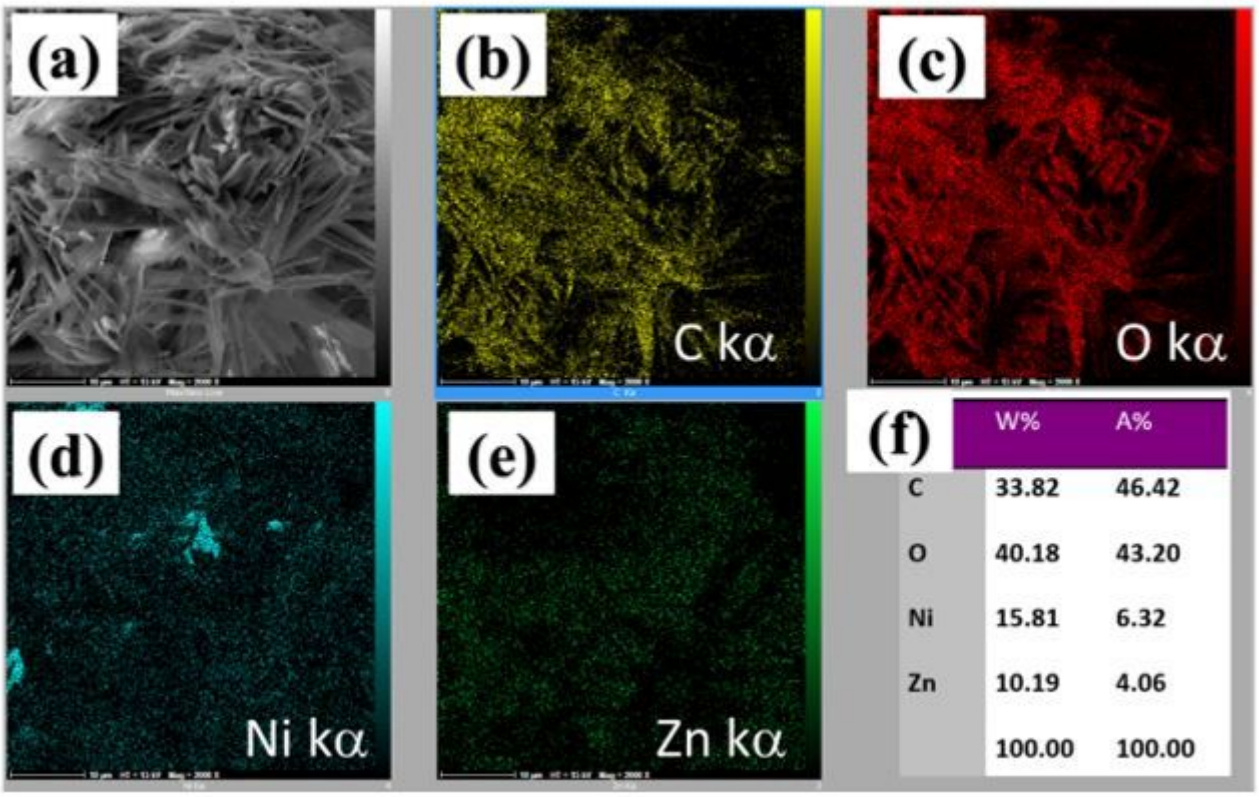

Figure 4

(a-d) Elemental mapping profiles and (e) EDX data of Ni,Zn-MOF/Ni foam electrode.

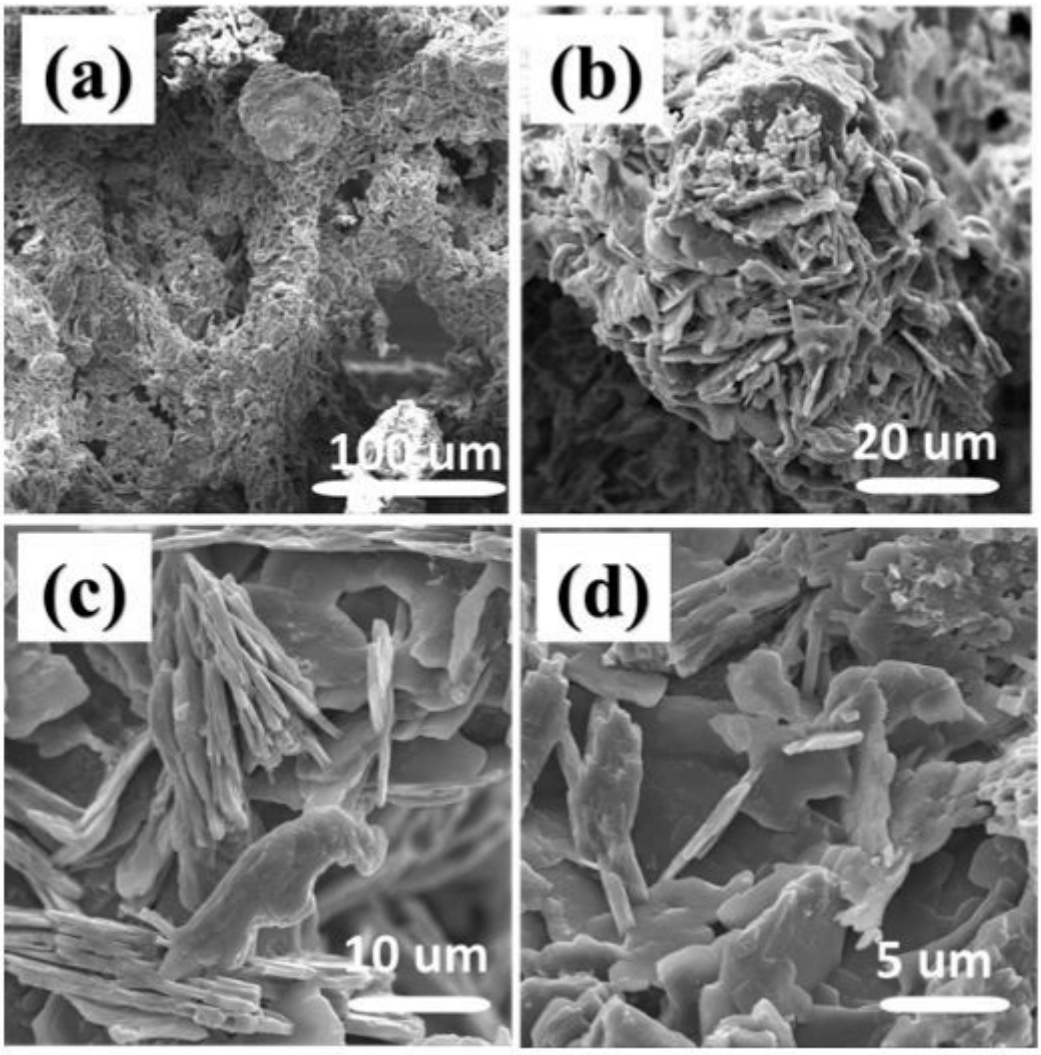

Figure 5

FE-SEM images of the MOF-derived hydroxide onto Ni-foam support.

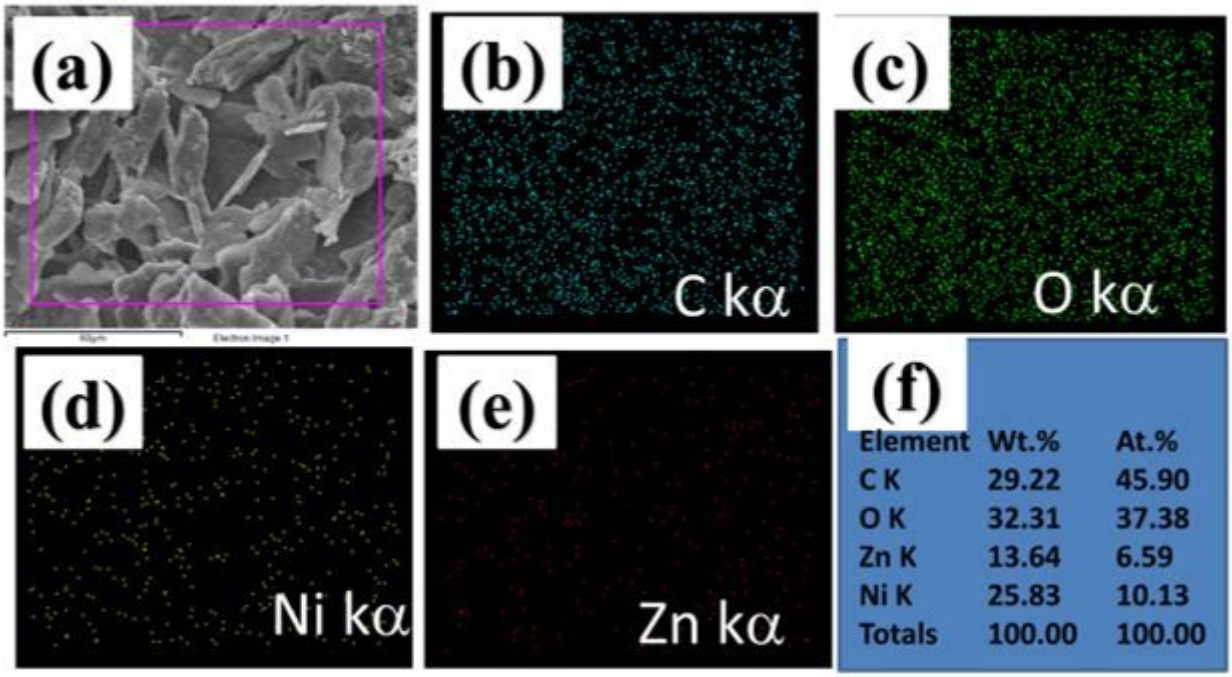

Figure 6

(a-d) Elemental mapping profiles and (e) EDX data of MOF-derived hydroxide@C/Ni foam electrode.

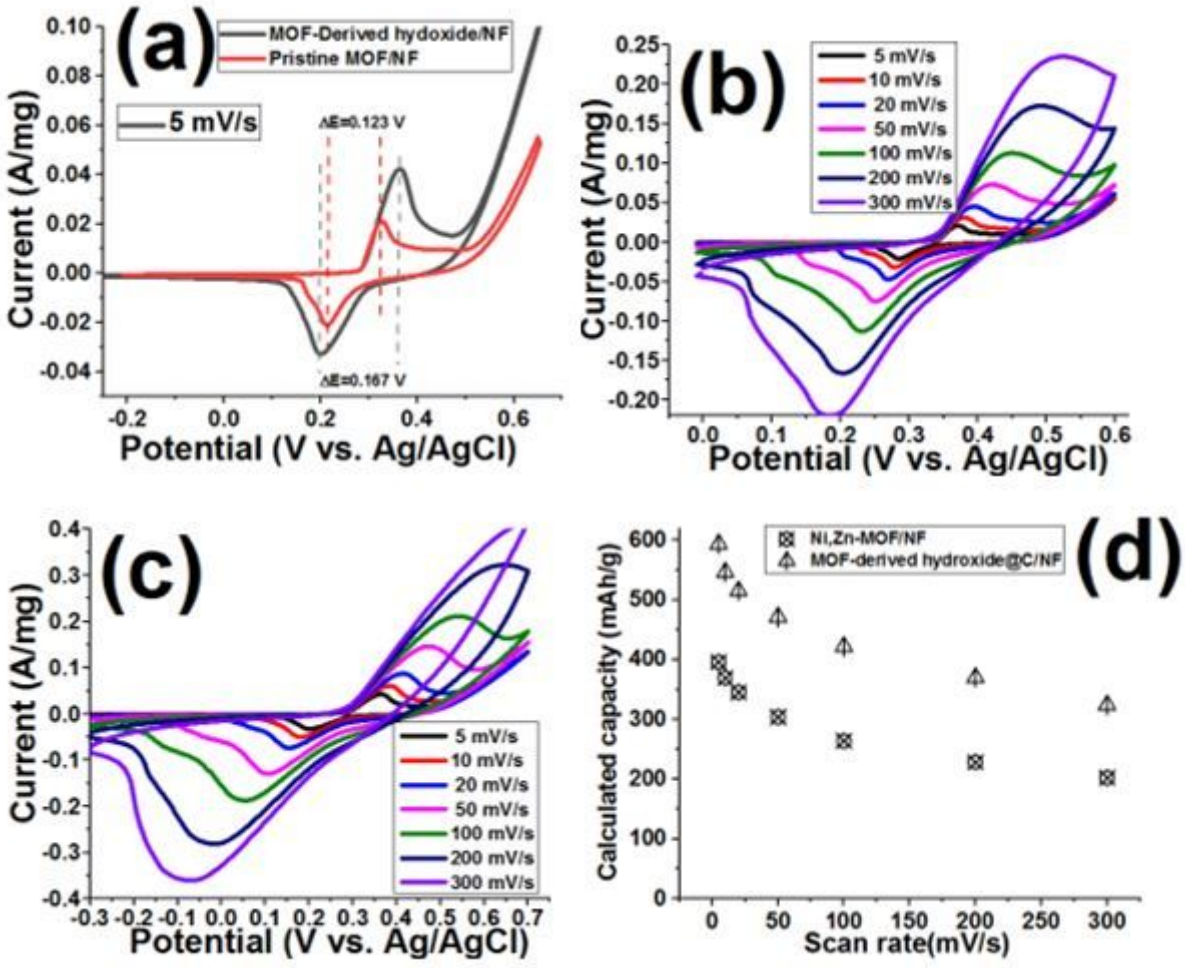

Figure 7

(a) CV curves of the fabricated Ni,Zn-MOF/Ni foam and its derived hydroxide/Ni foam electrodes at the scan rate of 5 mV/s, and (b,c) their CVs and (d) calculated capacitances at the different scan rates.

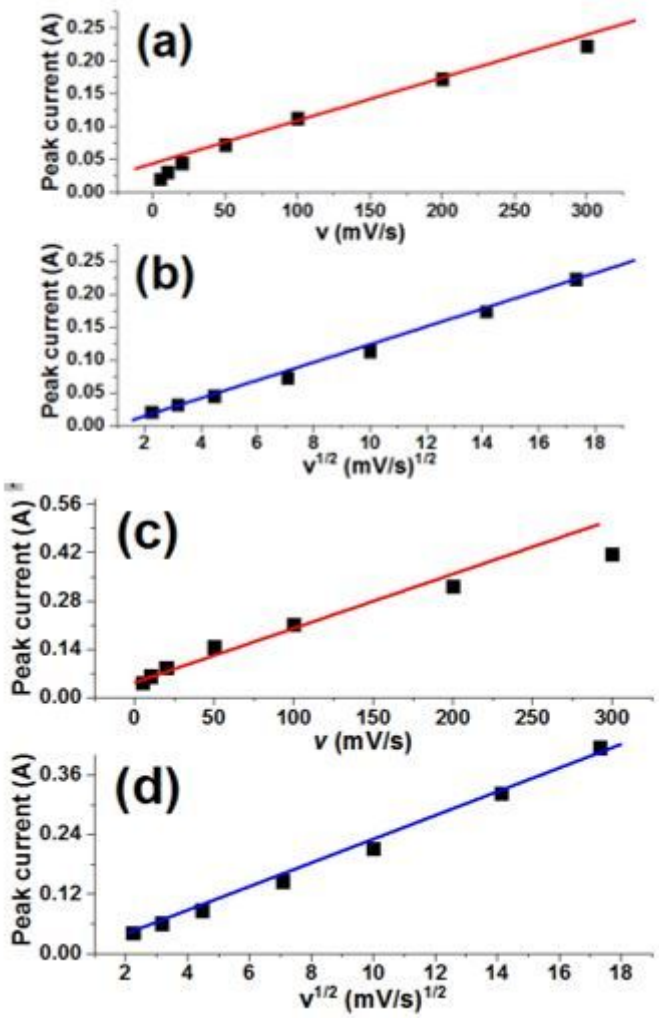

Figure 8

Peak current versus v and v1/2 for the fabricated (a,b) Ni,Zn-MOF/Ni foam and (c,d) MOF-derived hydroxide@C/Ni foam electrodes.

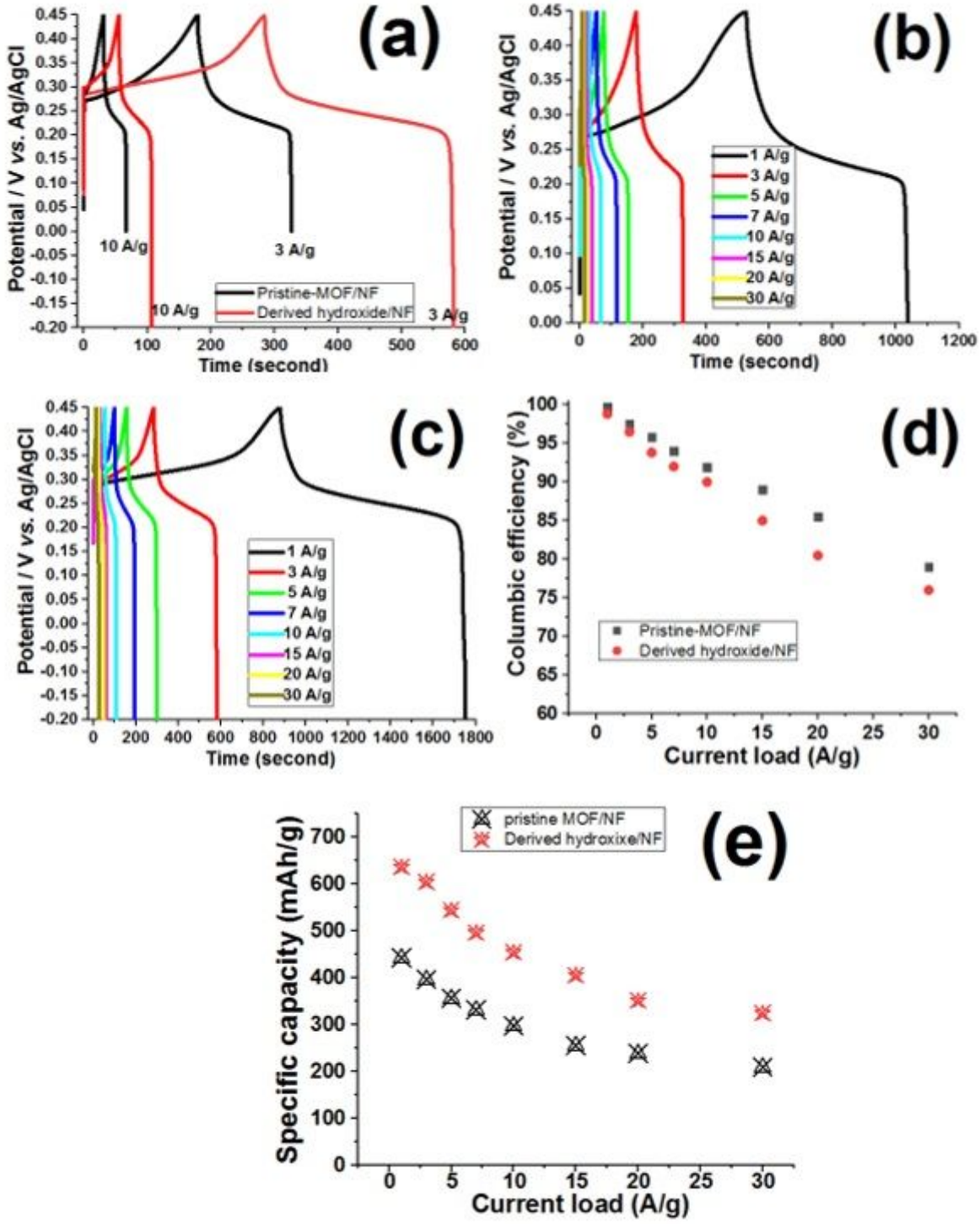

Figure 9

(a) GCDs of the fabricated Ni,Zn-MOF/Ni foam and its derived hydroxide/Ni foam electrodes at the current loads of 3 and 10 A/g, and (b,c) their GCDs, (d) faradic efficiency and (e) the calculated specific capacitance values m at the different current loads.

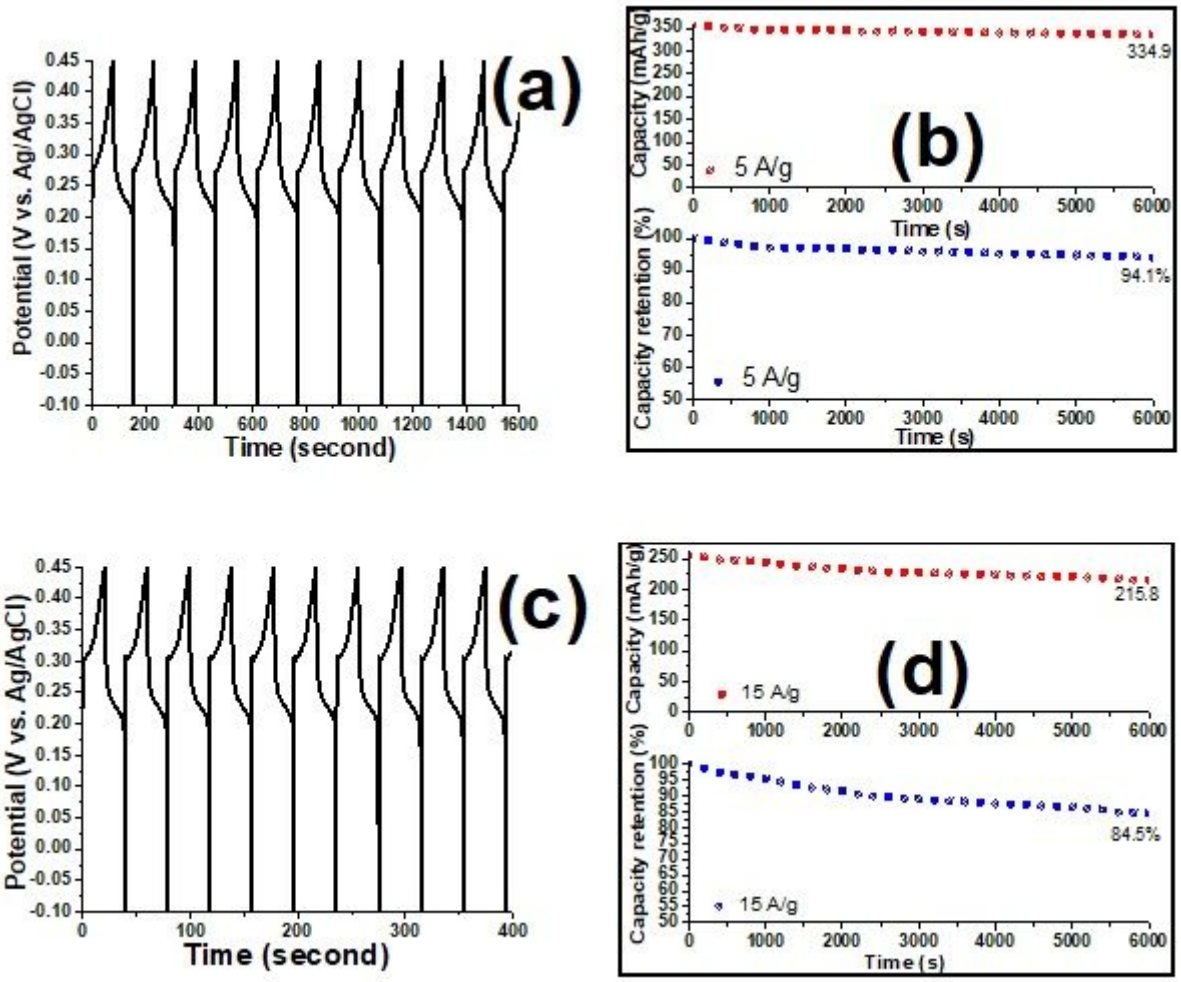

Figure 10

Cycling data of the fabricated Ni,Zn/MOF@Ni foam electrode at the applied current loads of (a,b) 5 A/g and (c,d) 15 A/g.

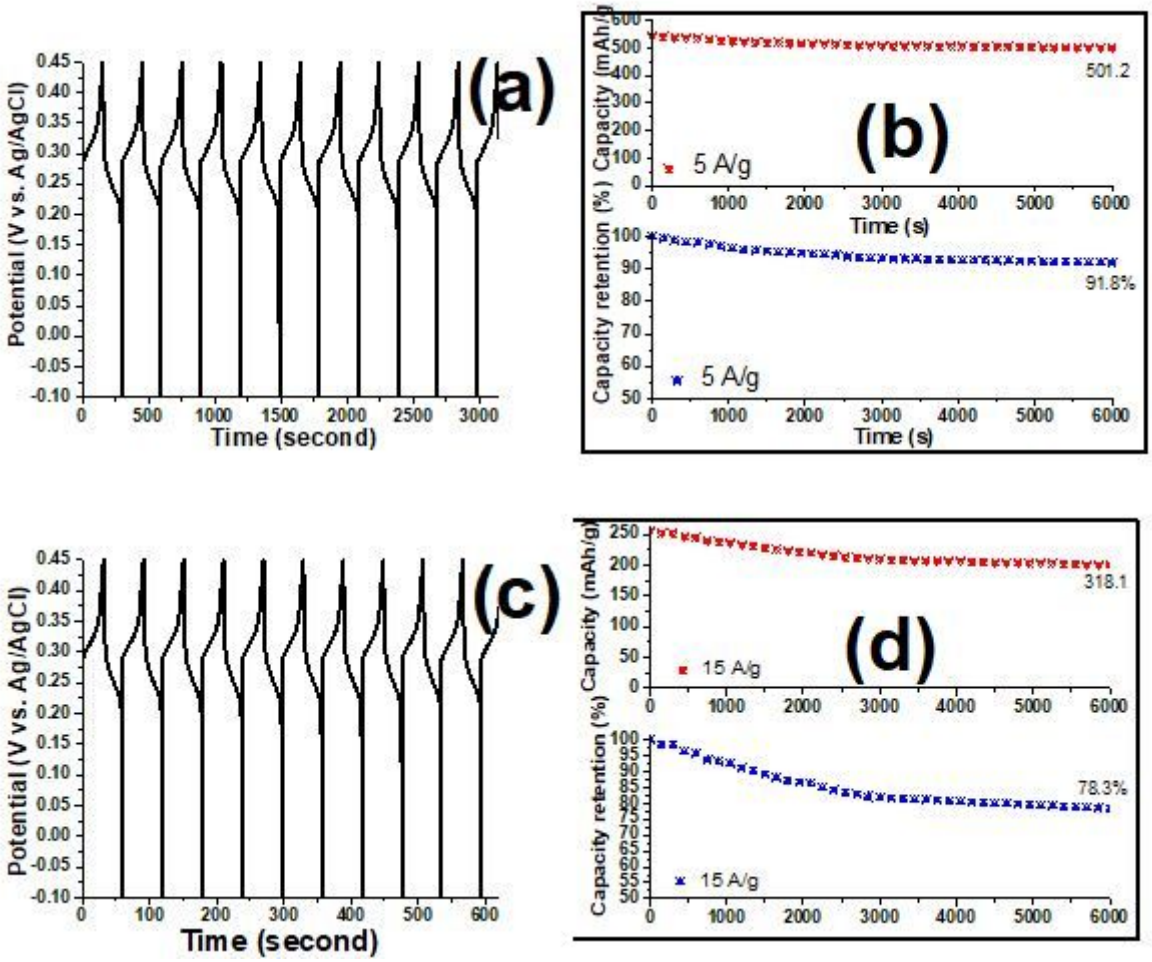

Figure 11

Cycling data of the fabricated MOF-derived hydroxide/Ni foam electrode at the applied current loads of (a,b) 5 A/g and (c,d) 15 A/g.

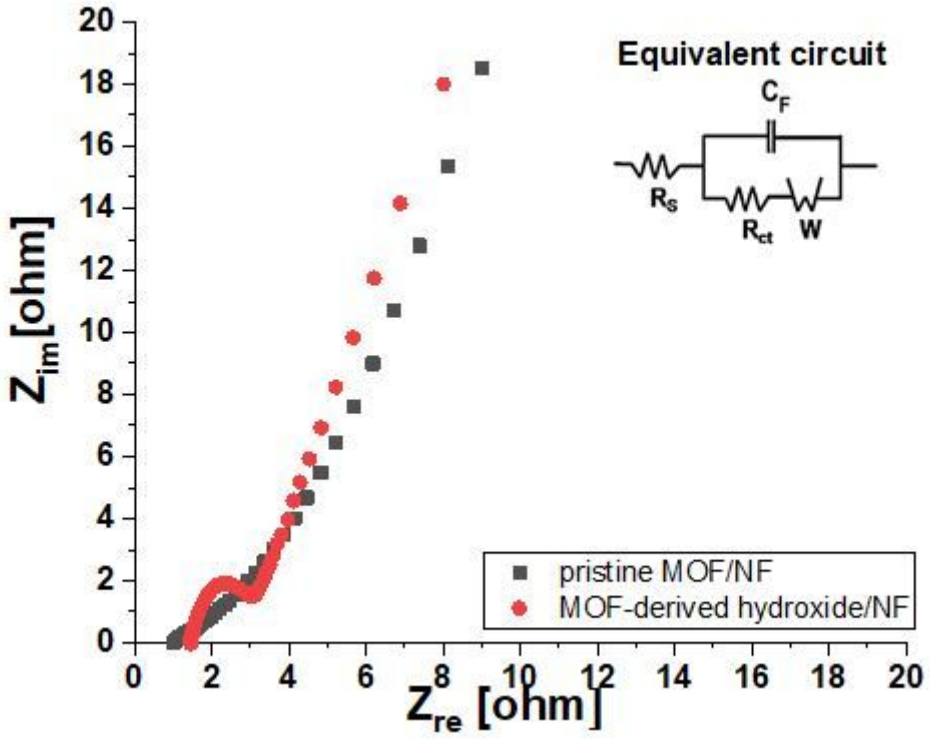

Figure 12

Nyquist plots for the fabricated electrodes at the frequency range of 100 kHz to 0.01 Hz. The insets show high-frequency zone and proposed equivalent circuit.